

Repair of Continuous Beams Pre-Damaged by Corrosion in Sagging Regions with C-FRCM Composites

Youssef Elmezayen¹, Tamer El-Maddawy²

¹PhD Candidate, College of Engineering, UAE University, UAE

²Professor, College of Engineering, UAE University, UAE

Article info

Article history:

Received 18 June 2023

Accepted 27 August 2023

Keywords: Concrete, Continuous, Corrosion, Flexure, FRCM, Repair

Abstract

Numerical models were developed to simulate the nonlinear structural behavior of flexure-deficient continuous reinforced concrete (RC) beams repaired with carbon fabric-reinforced cementitious matrix (C-FRCM) composites. Laboratory tests of large-scale continuous RC beams were conducted to validate predictions of the numerical models. A parametric study was performed to examine the effect of varying the elastic modulus of the fabric and the bonding condition at the fabric-mortar interface on the flexural response. Predictions of the numerical models were in good agreement with those obtained from the experiments. The difference between the predicted and experimental load capacities was within 10%. Results of the numerical analysis indicated that a 25% corrosion in the middle third of the sagging regions reduced the load capacity by 14%. The C-FRCM repair solution fully restored the original load capacity of the beam model. The use of the design value of the fabric's elastic modulus rather than the nominal value resulted in a numerical prediction closer to the response obtained from the experiment. The inclusion of a bond-slip law between the fabric and mortar in the numerical analysis was crucial to simulate the behavior of the corroded-repaired beam with good accuracy.

1. Introduction

Corrosion of steel reinforcing bars in RC beams results in rust stains, concrete cracks, a loss of reinforcement cross-sectional area, and a deterioration of bond between steel and the surrounding concrete [1]. The reduction in the load-carrying capacity caused by corrosion in simply-supported beams with well-anchored reinforcement is almost the same as the reduction in the moment strength of the midspan section [2-3]. In contrast, the load-carrying capacity of continuous RC beams is function of the moment strength of both sagging and hogging sections, and therefore a reduction in the moment strength in one location due to corrosion does not necessarily produce a similar reduction in load-carrying capacity of the beam. Due to their redundancy, continuous RC beams have the capacity to redistribute the moments between the damaged and undamaged critical sections, so that the formation of one plastic hinge does not necessarily lead to a structural collapse [4]. As such, continuous RC beams can withstand higher levels of corrosion damage than simply-supported

beams do, and therefore more time between the first symptoms of corrosion and the eventual collapse may elapse [4]. Fabric-reinforced cementitious matrix (FRCM) composites, consist of nonmetallic reinforcing fibers, such as carbon (C), glass (G), and Polyparaphenylene Benzobis Oxazole (PBO) surrounded by a cementitious matrix [5]. The inclusion of nonmetallic fiber strands and the use of a cement-based matrix improves the durability and heat resistance of the strengthening solution [5]. Consequently, FRCM composites have a great potential to repair flexure-deficient RC beams, particularly those exposed to corrosive environments. Despite their scarcity, previous studies on the rehabilitation of corrosion-damaged simply-supported RC beams provided interesting findings and conclusions [6-7]. Rehabilitation of a simply-supported RC beams with 13-22% corrosion in the flexural reinforcement using C-FRCM or PBO-FRCM composites fully restored the original load-carrying capacity of the virgin uncorroded beam [6-7]. Beams repaired with

FRCM typically failed by interfacial debonding at the fabric-mortar interface after yielding of the tensile steel reinforcing bars [6-7]. Although the strength gain caused by PBO-FRCM repair solutions was less pronounced than that produced by C-FRCM composites, the ductility of the beams repaired with former was greater than those repaired with the latter [7]. Dissimilar to the behavior of simply-supported beams, the flexural load-carrying capacity of continuous beams is governed by the rotational and moment capacities of the critical sections at both sagging and hogging regions. As such, data reported in the literature on the flexural behavior of deficient simply-supported RC beams repaired with FRCM composites are invalid for continuous structures. Providing data on the flexural behavior of continuous RC beams repaired with FRCM composites is crucial since practical applications would involve the flexural rehabilitation of continuous structural elements rather than simply-supported beams. This research aims to fill this gap through numerical modeling and experimental testing. The numerical predictions were validated through a comparative analysis with laboratory test results. A parametric study was then conducted to examine the effect of varying the elastic modulus of the fabric and the bonding condition at the fabric-mortar interface on the flexural response of the beams.

2. Model Development

Three-dimensional (3D) numerical models were developed using the software ATENA [8] to simulate the nonlinear behavior of corroded continuous RC beams before and after repair with C-FRCM composites. Three continuous beam models were initially developed. One model did not have a deficiency to act as a benchmark, whereas the other two models had deficiency of 25% corrosion in the middle third of the sagging region. One of the flexure-deficient beam models was repaired with FRCM composites, while the other was kept unrepaired.

Configuration of the Continuous Beam Model

Figure 1 shows details of the continuous beam models. The models had a total length of 5200 mm and two equal spans, 2400 mm each. The cross-section of the beam models had a width of $b = 150$ mm, depth of $h = 250$ mm, and an effective depth of tension steel of $d = 225$ mm. The beams were designed according to the ACI 318-19 [9] to fail in flexure. The tensile steel in both sagging and hogging regions consisted of three 12 mm diameter steel bars, while the compressive steel included two 6 mm diameter bars. The tensile steel in the hogging region had a total length of 1600 mm. Steel stirrups with a diameter of 8 mm were used at a spacing of 75 mm. The deficient beam models had a 25% corrosion in the middle third of each sagging region. The cube and cylinder compressive strengths of the concrete were 40 and 29, respectively, whereas its splitting tensile strength was 2.4 MPa. The tensile steel had yield and ultimate strengths of 561 and 649 MPa, respectively. The yield strength of the stirrups and the compressive steel was 525 MPa. The C-FRCM

repair scheme is shown in Figure 2. It involved the installation of one 1500 mm long near-surface-embedded (NSE) C-FRCM layer placed symmetrically around the load point, and one externally-bonded (EB) C-FRCM layer covering approximately 90% of the span. Each FRCM composite layer included one carbon fabric sheet embedded into a mortar layer with a thickness of about 8 mm. The fabric comprised unidirectional carbon fiber strands with a spacing of 17 mm. The physical appearance of a typical carbon fabric sheet along with its main characteristics, provided by the manufacturer [10], are given in Table 1. The cube and cylinder compressive strengths of the mortar were 45 and 35 MPa, respectively, while its respective splitting tensile strength and Young's modulus were 3.4 MPa and 28 GPa.

Material Constitutive Laws

Material constitutive laws that account for the nonlinear behavior of materials and the bonding conditions between the reinforcement and surrounding matrix were adopted. The nonlinear behavior of the cementitious materials in compression starts at a compressive stress value of $f'_{co} = 2f_t$, where f_t is the uniaxial tensile strength, assumed as 0.67 of the splitting tensile strength. The compressive stress (σ_c) during the hardening phase is linked to the plastic strain (ε_p) through a nonlinear function [11], until the cylinder compressive strength (f'_c) is reached (Figure 3a). The value of the plastic strain at peak (ε_{cp}) is generated automatically by the software, based on the concrete cube strength. The compressive stress decreases linearly in the post-peak phase as function of the compressive displacement (w_c) through the length scale L_c (Figure 3b). The compressive displacement at a complete release of stress (w_d) equals to 0.5 mm [8]. The tensile stress (σ_t) softening law exhibits an exponential function based on the crack opening displacement (w_t) through the length scale L_t (Figure 3c). The software determines the crack opening at zero stress (w_{tc}) based on f_t and the fracture energy (G_f) of the material. The tension steel bars were modeled as linear-elastic with a post-yield strain hardening of 1%. An elastic-perfectly plastic behavior was assumed for the stirrups and compressions steel. The carbon fiber strands had a linear-elastic behavior till failure. A perfect bond was assumed between the mortar and concrete substrate. The bond-slip law adopted between the steel and concrete is shown in Figure 4a [11], whereas that adopted at the fabric-mortar interface is depicted in Figure 4b [12]. It is noteworthy that only 50% of the perimeter of each fiber strand was considered in the numerical analysis as a conservative assumption due to the difficulty in determining the exact surface area of the fiber strands that contributes to the bond resistance.

Element Types and Boundary Conditions

Solid macro-elements, with a maximum mesh size of 25 mm, were used to simulate the concrete beam, mortar layers, and steel plates. The steel reinforcing bars and the carbon fiber strands were simulated by one-dimensional discrete elements embedded into the concrete and mortar macro-elements, respectively.

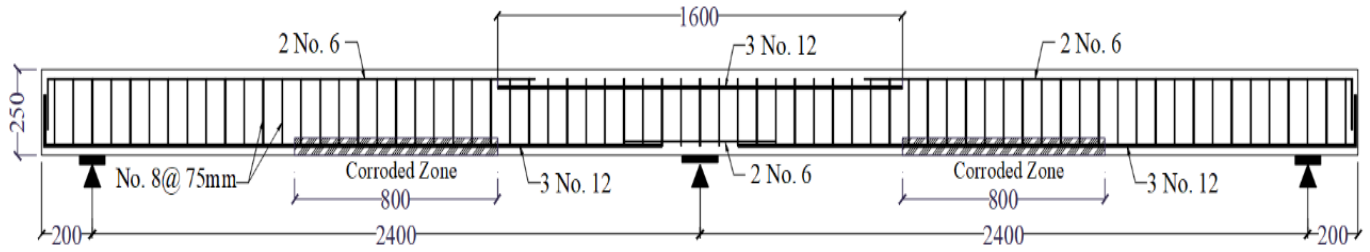


Fig. 1: Geometry and Details of Reinforcement

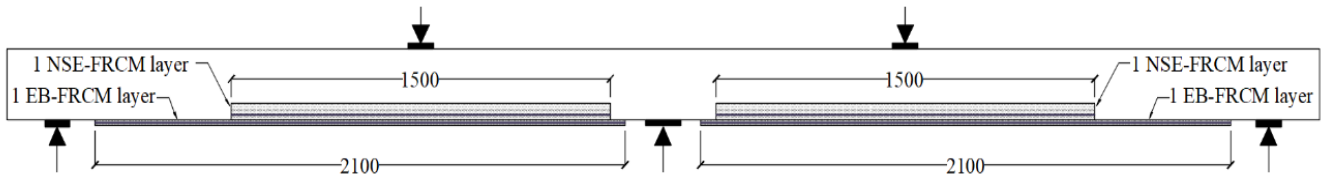



Fig. 2: FRCM Repair Scheme

Table 1: Characteristics of the carbon fabric

Property	Image/Value
Physical appearance	
Cross-sectional area (mm ² /mm)	0.157
Spacing between fiber strands (mm)	17.0
Modulus of elasticity (GPa)	240 (160)*
Elongation at break (%)	1.80

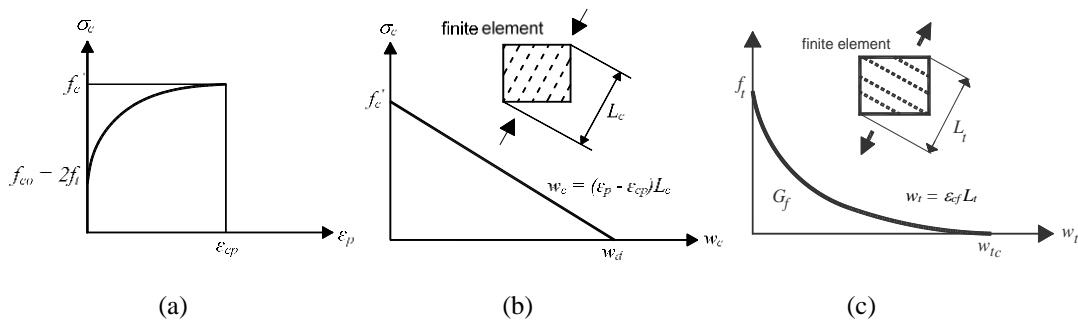


Fig. 3: Cementitious Material Constitutive Laws; (a) Compressive Hardening, (b) Compressive Softening, (c) Tensile Softening

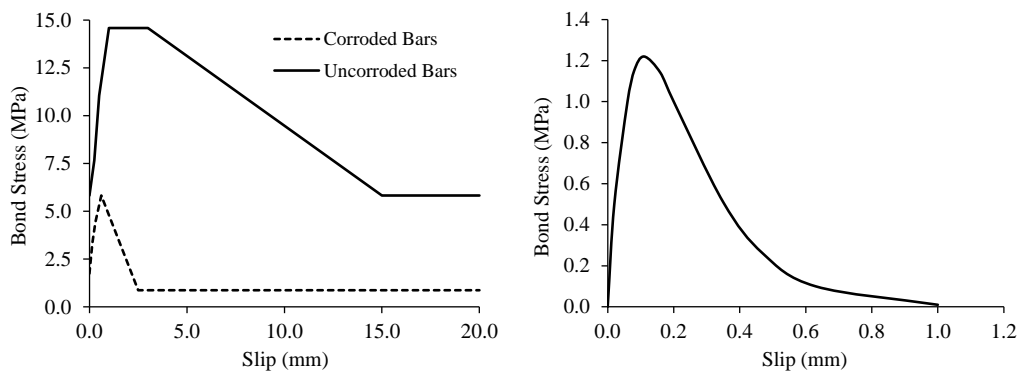


Fig. 4: Bond-Slip Laws; (a) Steel-Concrete Interface [11], (b) Fabric-Mortar Interface [12]

Half of the beam was modeled to benefit from the symmetry at the central support. The end and central support plates were restricted from movement in the vertical and transverse directions. Surface supports were used to prevent the movement in the longitudinal direction at the plan of symmetry. Prescribed displacements were induced at the midpoint of the loading plate at a rate of 0.1 mm/step. Figure 5 shows elements and boundary conditions of a typical half-numerical model with FRCM. The software adopts the standard Newton-Raphson iterative solution in the analysis. The iterations of each time step end when a specific convergence criterion pertaining to compatibility of displacements, equilibrium of forces, and balance of energy is satisfied.

Modeling of Corrosion

Corrosion of steel in concrete reduces the area of the reinforcing bars and impairs the bond between the steel and surrounding concrete. The impacts of corrosion of steel in RC beam models pre-damaged by corrosion in the tension zone can be considered through a reduction in the cross-sectional area of the deficient steel reinforcing bars and a change in the bond-slip law at the steel-concrete interface. The cross-sectional of the tensile steel reinforcing bars located in the corroded zone of the flexure-deficient beam models was 75% of that of the uncorroded bars located outside the corroded region to account for the 25% reduction in the steel area caused by corrosion. Furthermore, the bonding condition at the steel-concrete interface for the corroded-unrepaired beam model was changed from good to poor [8,11]. Such a change in the bond behavior affected the bond-slip law adopted in the analysis (refer to Figure 4a).

3. Model verification

The virgin beam was constructed and tested previously by the second author's research group [13]. Additional two beams were fabricated then subjected to accelerated corrosion by means of an impressed current technique. The C-FRCM repair process is summarized in Figure 6. The repair works included edge conditioning, removal of deteriorated concrete, undercutting of exposed bars, surface cleaning of steel, roughening of the concrete substrate, and placement of FRCM composite layers. The cementitious mortar was applied first on the concrete substrate to fill the space behind the corroded steel and sufficiently cover the exposed stirrups. One NSE C-FRCM composite layer was then installed within the thickness of the clear cover followed by the application of the EB C-FRCM layer. The repaired area was moist-cured using wet burlaps for 28 days. The test setup is shown in Figure 7. The specimens were placed on three supports, 2400 mm apart. A 500 kN capacity MTS actuator was used to apply the load at the midpoint of the beam that was spread equally on two points, by means of a rigid steel beam. Each of the loading points was located at a distance that corresponded to 40% of the beam span, measured from the central support. A load cell was placed between the actuator and the top surface of the steel spreader beam to measure the total applied load. Another load cell was placed between the central support and the

bottom surface of the beam to measure the central support reaction. Two linear variant displacement transducers (LVDTs) were used to measure the beam deflection at the bottom surface below the loading points.

A comparative analysis between the numerical and experimental test results was conducted. The load deflection responses predicted numerically are compared to those obtained from the tests in Figure 8, noting that the design value of the fabric's elastic modulus (160 GPa) was considered in the numerical analysis. The numerical and experimental load-deflection responses were, generally, in good agreement. The numerical prediction of the control beam indicated the occurrence of the first yielding in the hogging region followed by a second yielding in the sagging region, which was in alignment with the experimental results. Corrosion of the steel bars in the sagging region reduced the difference between the sagging and hogging yield loads predicted numerically, since yielding of the steel in the sagging region occurred rapidly after it happened in the hogging. Nevertheless, the experimental response of the corroded-unrepaired beam indicated the occurrence of the first yielding in the sagging region followed by a second yielding in the hogging region. Following yielding of steel reinforcement in both sagging and hogging regions, the unstrengthened beam models exhibited almost a plastic response until failure, which was consistent with the experimental response. The corroded-repaired beam model exhibited first yielding at the hogging region followed rapidly by yielding of steel bars in the sagging region, although experimental observations indicated the occurrence of steel yielding at both regions almost concurrently. The difference between the numerical and experimental results of the corroded beams related to the order of the steel yielding could be ascribed to a variation between properties of the tested steel coupons and those of the actual steel bars used in the construction of the tested beams. The corroded-repaired beam exhibited a hardening response after yielding of the steel reinforcement. The repaired beam showed a sudden drop at peak load, probably due to an interfacial debonding at the fabric-mortar interface followed by a plastic response until a complete failure of the beam occurred. The predicted and experimental ultimate loads of the beams are compared in Table 2. The difference between the numerical and experimental ultimate loads was within a 10% error band. Such a difference could be considered within the acceptable margin of error. The numerical results indicated that a 25% corrosion in the sagging region reduced the load capacity of the beam model by 14%. The C-FRCM repair solution fully restored the load capacity of the virgin beam. The effectiveness of the C-FRCM repair solution to fully restore the original load capacity was predicted numerically and verified experimentally.

4. Parametric study

Three additional continuous beam models with C-FRCM reinforcement were created to study the effect of varying the elastic modulus of the fabric and the bonding condition at the fabric-mortar interface on the flexural behavior of corroded-repaired beam models.

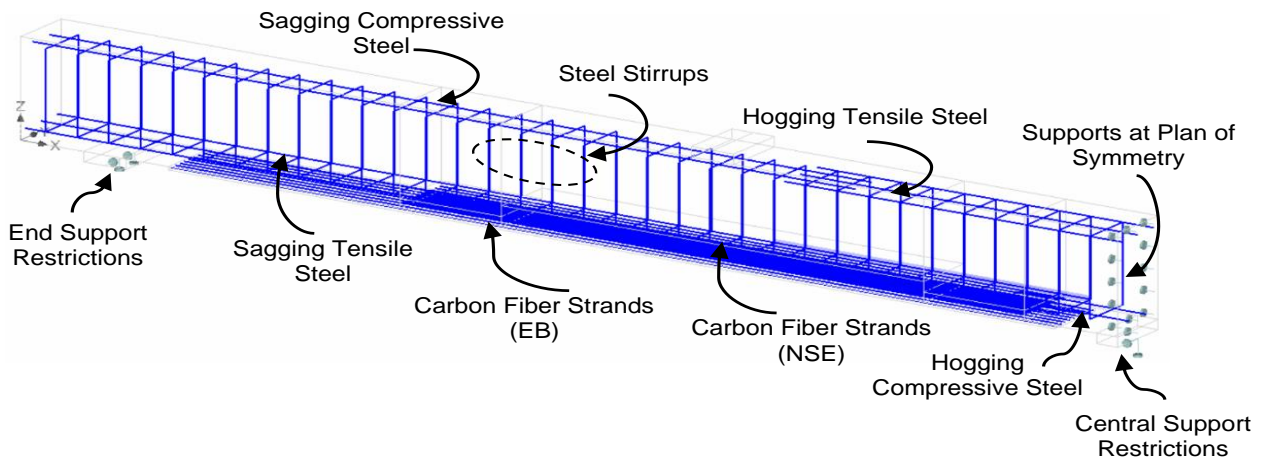


Fig. 5: Typical Numerical Model

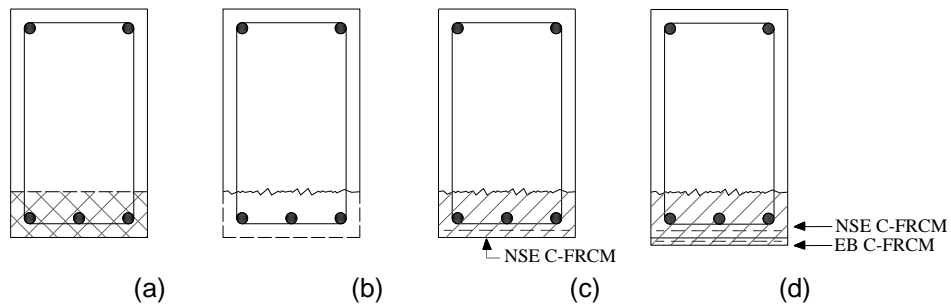


Fig. 6: C-FRCM Repair Process; (a) Identification of Damaged Areas, (b) Removal of Deteriorated Concrete, Cleaning of Steel, and Surface Preparation, (c) Application of Mortar and NSE C-FRCM Layer; (d) Application of EB-FRCM Layer

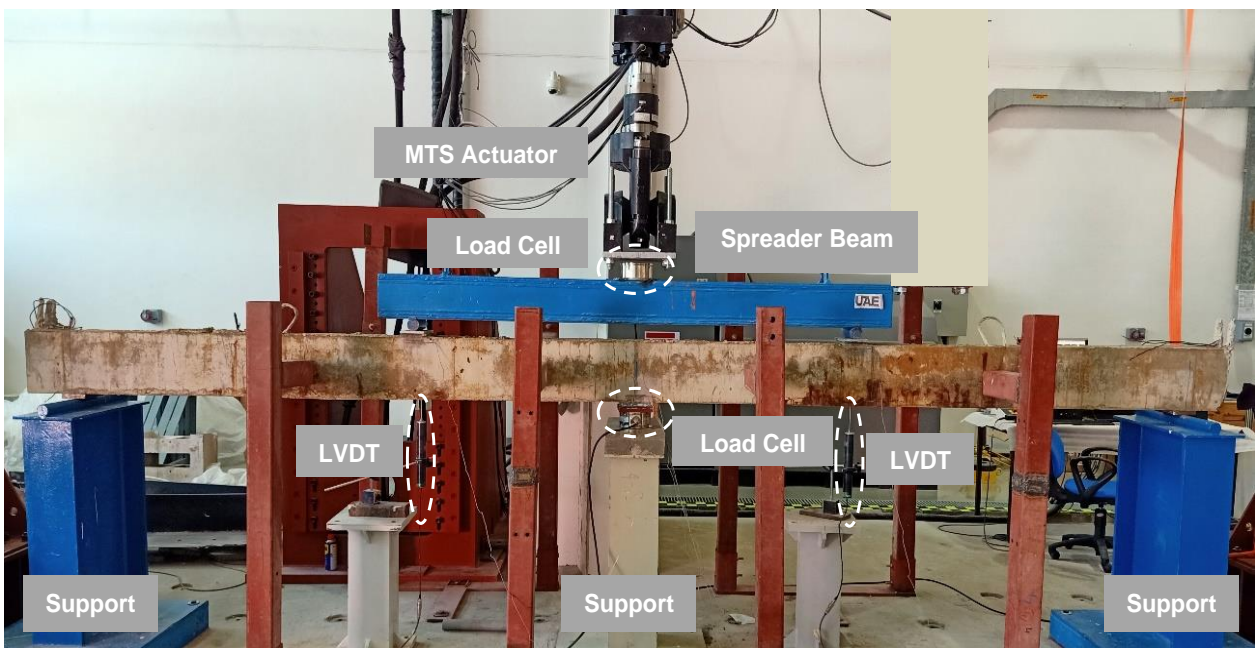


Fig. 7: Test Setup

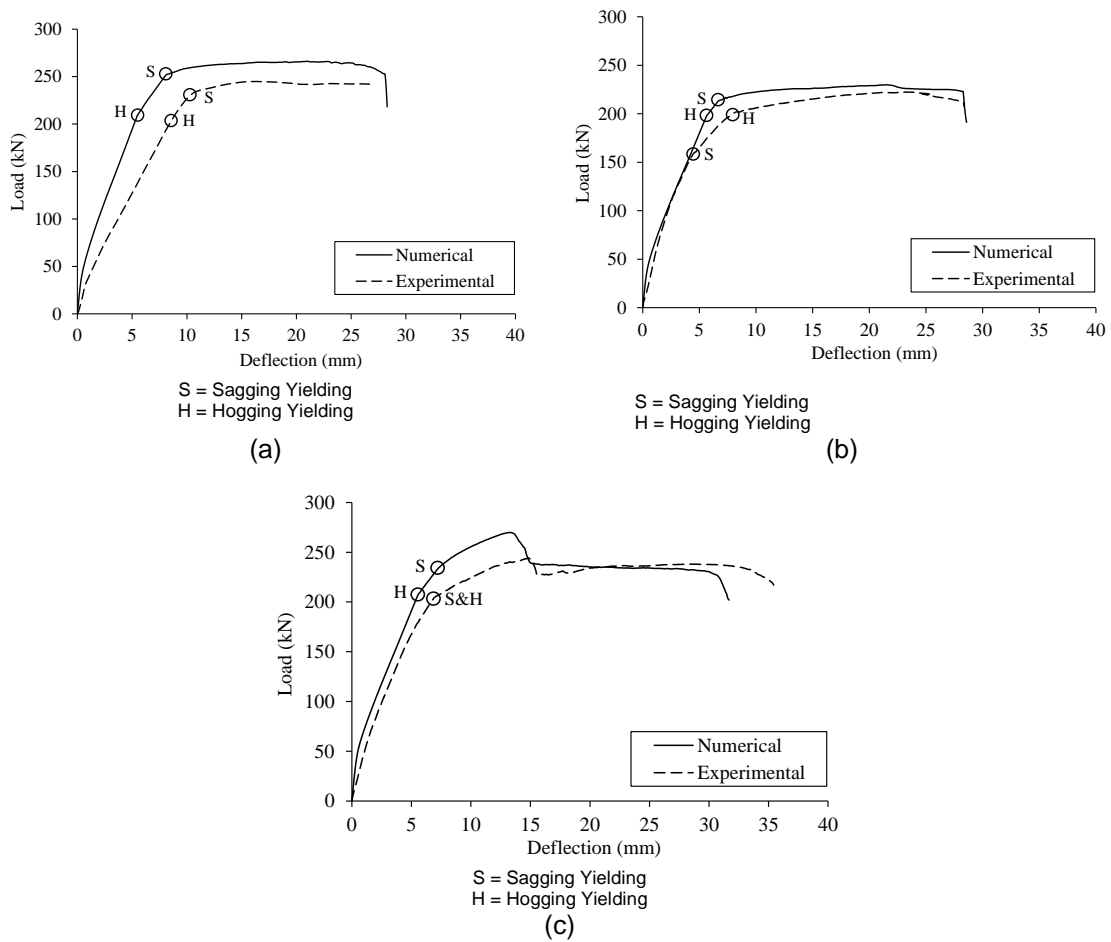


Fig. 8: Load-Deflection Response; (a) Control, (b) Corroded-Unrepaired, (c) Corroded-Repaired

Table 2: Numerical versus experimental results

Notation	Ultimate Load (kN)		Error (%)*
	Numerical	Experimental	
Control	266.2	244.8	9
Corroded-Unrepaired	229.8	222.3	3
Corroded-Repaired	269.8	244.5	10

$$*Error (%) = \frac{\text{Numerical-Experimental}}{\text{Experimental}} \times 100$$

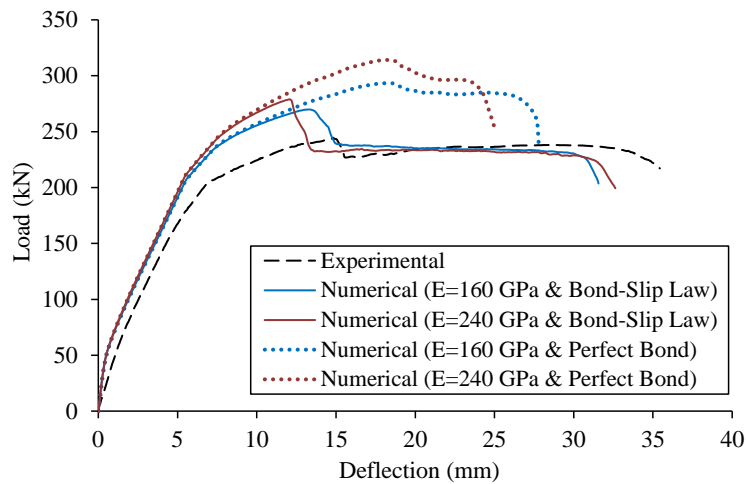


Fig. 9: Effect of Varying the Fabric's Elastic Modulus and Bonding Condition on the Flexural Response

Figure 9 shows the load-deflection responses predicted numerically for the models with FRCM reinforcement along with the response obtained from the test. The use of the nominal elastic modulus of the fabric (240 GPa) rather than the design value (160 GPa) slightly increased the post-yield stiffness of the beam models. Furthermore, the ultimate loads of the beam models with the higher fabric's elastic modulus of 240 GPa were 3 to 7% higher than those of their counterparts with the lower fabric's elastic modulus of 160 GPa. The adoption of the perfect bond assumption at the fabric-mortar interface in the numerical analysis resulted in a higher ultimate load and deflection capacity relative to those of the beam models with the bond-slip law at the fabric-mortar interface. Future research shall examine the effect of a wider range of parameters on the flexural response of corroded continuous RC beams repaired with FRCM composites, including different degrees and locations of corrosion damage.

5. Conclusions

Numerical simulation models were developed to predict the nonlinear behavior of flexure-deficient continuous RC beams before and after repair with C-FRCM composites. The accuracy of the numerical models was examined through a comparative analysis with results of continuous RC beams tested in the laboratory. A parametric study was conducted to investigate the flexural behavior of continuous RC beam models with several fabric's elastic moduli and bonding conditions at the fabric-mortar interface. Based on the results of the numerical analysis, the following conclusions can be drawn:

- The decrease in the load capacity of continuous RC beam models caused by corrosion in the sagging region was not the same as the reduction in the cross-sectional area of the corroded steel reinforcing bars.
- The load capacity of the corroded-unrepaired continuous RC beam model with a 25% corrosion in the sagging region was 14% lower than that of the virgin beam model.
- The rehabilitation of the corroded beam model with C-FRCM composites fully restored the original load capacity of the considered beam. The load capacity of the corroded-repaired beam model was 17% higher than that of the corroded-unrepaired beam model.
- Increasing the elastic modulus of the fabric from 160 to 240 GPa in the numerical analysis increased the load capacity of the corroded-repaired beam models with and without the bond-slip law at the fabric-mortar interface by 3 and 7%, respectively.
- The use of the perfect bond assumption at the fabric-mortar interface resulted in a higher ultimate load and a greater deflection capacity relative to those of the beam models with the bond-slip law at the fabric-mortar interface.
- The numerical models developed in the current study can be used as a numerical platform for

performance prediction of RC continuous beams repaired with FRCM composites.

The present study provided an insight into the effectiveness of using C-FRCM composites to improve the flexural response of two-span RC beams with 25% corrosion in the sagging regions. Future research should focus on investigating the flexural behavior of continuous RC beams repaired with several types of FRCM composites at various degrees of corrosion. The effect of varying the location of corrosion damage (sagging region, hogging region, and both regions simultaneously) on the flexural behavior of continuous RC beams before and after repair with FRCM composites should be investigated in future studies.

Acknowledgements

This research is funded by the United Arab Emirates University under grant number 12N004.

References

1. Soltani M., Safiey A., Brennan A. (2019), "A state-of-the-art review of bending and shear behaviors of corrosion-damaged reinforced concrete beams", *ACI Structural Journal*, Vol. 116, pp. 53–64.
2. El Maaddawy T., Soudki K., Topper, T. (2005), "Long-term performance of corrosion-damaged reinforced concrete beams", *ACI Structural Journal*, Vol.102, pp. 649–656.
3. A. Bossio A., Imperatore S., Kioumarsi M. (2019), "Ultimate flexural capacity of reinforced concrete elements damaged by corrosion", *Buildings*, Vol. 9, 160.
4. Fernandez I., Herrador M., Marí A., Bairán J. (2016), "Structural effects of steel reinforcement corrosion on statically indeterminate reinforced concrete members", *Materials and Structures*, Vol. 49, pp. 4959–4973.
5. ACI Committee 549. (2020), "Guide to design and construction of externally bonded fabric-reinforced and steel-reinforced grout systems for repair and strengthening of concrete structures (ACI 549.4R-20)", ACI, MI, USA.
6. El-Maaddawy T., El Refai A. (2016), "Innovative repair of severely corroded t-beams using fabric-reinforced cementitious matrix", *Journal of Composites for Construction*, Vol. 20, 04015073.
7. Elghazy M., El Refai A., Ebead U., Nanni A. (2018), "Corrosion-damaged RC beams repaired with fabric-reinforced cementitious matrix", *Journal of Composites for Construction*, Vol. 22, 04018039.
8. ATENA [Computer software]. (n.d.). Červenka Consulting s.r.o., Prague, Czech Republic. <https://www.cervenka.cz/products/atena/>.
9. ACI Committee 318. (2019), "Building code requirements for structural concrete—commentary on building code requirements for structural concrete (ACI 318R-19)", ACI, MI, USA.
10. S&P—A Simpson Strong-Tie Company. S&P ARMO-Mesh Reinforcement Made from Carbon Fiber. Available online: <https://www.sp-reinforcement.ch/en-CH>.

11. Comité Euro-International du Béton (1990), "CEB-FIP Model Code-Design Code", Thomas Telford, London, UK.
12. Abu Obaida F., El-Maaddawy T., El-Hassan H. (2021), "Bond behavior of carbon fabric-reinforced matrix composites: Geopolymeric matrix versus cementitious mortar", *Buildings* Vol. 11, 207.
13. Khattak N., Mansour M., El-Maaddawy T., Ismail, N. (2022), "Continuous reinforced concrete beams strengthened with fabric-reinforced cementitious matrix: experimental investigation and numerical simulation", *Buildings*, Vol. 12, 27.